Supporting Information

An ultra-stable Cu^{I}_{12} cluster built from a Cu^{I}_{6} precursor sandwiched by two Cu^{I}_{3}-thiacalixarene units for efficient photothermal conversion

Zuohu Zhou, Linmeng Xu, Guiyan Zhao,* Kun, Zhou, Baokuan Chen, Yanfeng Bi*

School of Petrochemical Engineering, Liaoning Petrochemical University, Fushun, Liaoning 113001 (P. R. China). E-mail: gyzhao@lnpu.edu.cn (G. Y. Zhao); biyanfeng@lnpu.edu.cn (Y. F. Bi)

ESI Contents

1 Experiment

1.1 Synthesis of $Cu^{I}_{6}(2\text{-PyS})_{6}$ (2-PySH = 2-Pyridinethiol)

A mixture of 2-Pyridinethiol (0.22 g, 2.0 mmol), CuCl (0. 20 g, 2.0 mmol), MeOH (5.0 mL), and DMA (5.0 mL) in a 20 mL Teflon-lined autoclave which was kept at 130 °C for one day and then slowly cooled to 20 °C. ca. 0.20 g red block crystals were obtained in 60.0% yield (basis on copper atom). The crystals were isolated by filtration and then washed with 1:1MeOH-DMA and dry in air.

1.2 Chemical stability of Cu_{12}

Cu_{12} is ultra-stable in the air by comparing the PXRD patterns from single-crystal X-ray diffraction (SCRD) with that exposure for 6 months. We also tested the stability of **Cu_{12}** under different conditions. We soaked **Cu_{12}** in 1 M HCl or 1 M NaOH for 48h or soaked it in 1 M H_2O_2 solution for 6h. Furthermore, we soaked freshly prepared **Cu_{12}** in various solvents for 48 h, including DMA, acetonitrile, acetone, dichloromethane, trichloromethane, methanol, ethanol, and mixed solvent (DMA: ethanol=1:1). The crystallization of **Cu_{12}** is maintained well, suggesting the outstanding stability of **Cu_{12}** in water solutions and various organic solvents.

1.3 Density functional theory (DFT) calculations

The model structure was obtained from single-crystal X-ray diffraction. The structure was optimized in Gaussian 16 program (Gaussian 16, Revision C. 01. Gaussian, Inc., Wallingford CT. 2016) with B3LYP functional,[1] def2-SVP base set,[2] and DFT-D3 dispersion correction.[3] Multiwfn, a multifunctional wave function analysis program[4], is used to generate the lattice file of molecular orbitals, and the three-dimensional graph is drawn by the VMD program.[5]

1.4 Solid photothermal experiment:

The light source is a 660 nm laser, with a light intensity of 0.4 W•cm^2. The sample was made into 1 cm^2 slice on 2.0 × 2.0 cm^2 glass sheets, and the distance between the laser lamp and the sample was changed to make the spot completely coincide with the sample. The temperature of the sample was measured by FL-IR infrared thermography. The test environmental conditions are kept at ca. 20 °C and humidity 30 %.

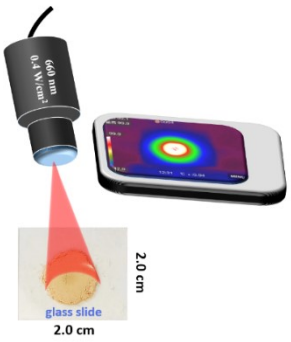

Diagram of the photothermal experiment for solid

1.5 Solvent photothermal experiment:

Add 15 mg of the **Cu_{12}** to 0.5 mL of H_2O or DMF, and the solid **Cu_{12}** was irradiated under a 660 nm laser with a power density of 0.4 W/cm^2, and the temperature was recorded by a thermal imager.

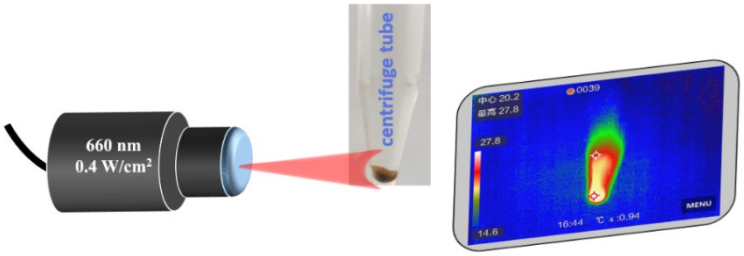

Diagram of the photothermal experiment in solvent

References

1 T. Yanai, D. P. Tew and N. C. Handy, A new hybrid exchange-correlation functional using the Coulomb-attenuating method (CAM-B3LYP), *Chem. Phys. Lett.*, 2004, **393**, 51–57.

2 F. Weigend and R. Ahlrichs, Balanced basis sets of split valence, triple zeta valence and quadruple zeta valence quality for H to Rn: Design and assessment of accuracy *Phys. Chem. Chem. Phys*., 2005, **7**, 3297.

3 S. Grimme, Density functional theory with London dispersion corrections, *WIREs Comput Mol Sci,* 2011, **1**, 211–228.

4 T. Lu and F.-W. Chen, Multiwfn: A multifunctional wavefunction analyzer, *J. Comput. Chem*., 2012, **33**, 580–592.

5 W. Humphrey, A. Dalke and K. Schulten, VMD: Visual molecular dynamics *J. Mol. Graph. Model*., 1996, **14**, 33–38.

Figures

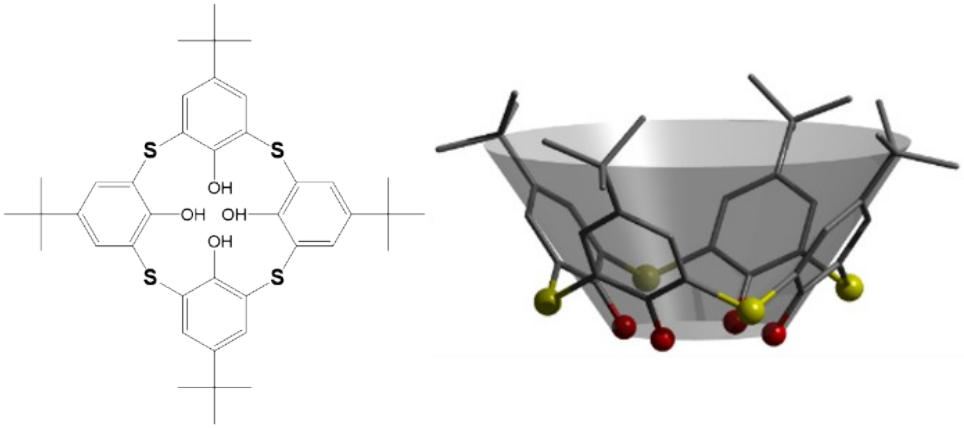

Fig. S1 *p-tert*-Butylthiacalix[4]arene (H_4TC4A)

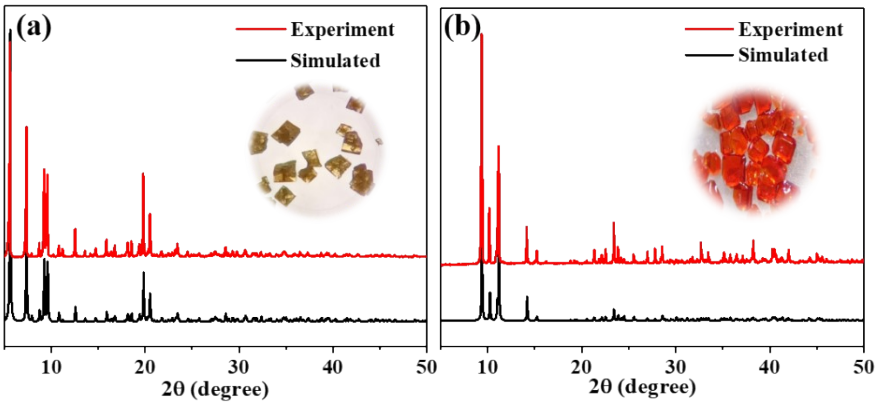

Fig. S2 (a) The PXRD patterns of $\mathbf{Cu_{12}}$. (b) The PXRD patterns of $\mathbf{Cu_6}$.

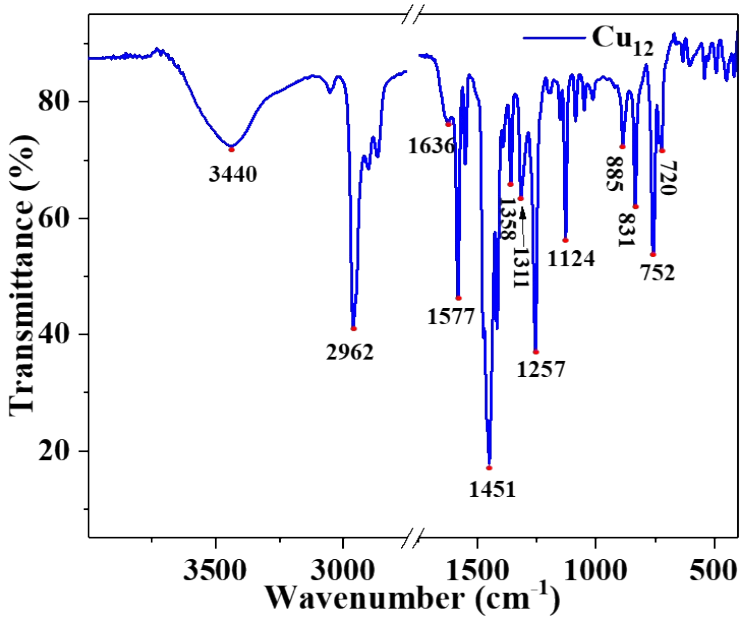

Fig. S3 FT-IR spectra of the $\mathbf{Cu_{12}}$

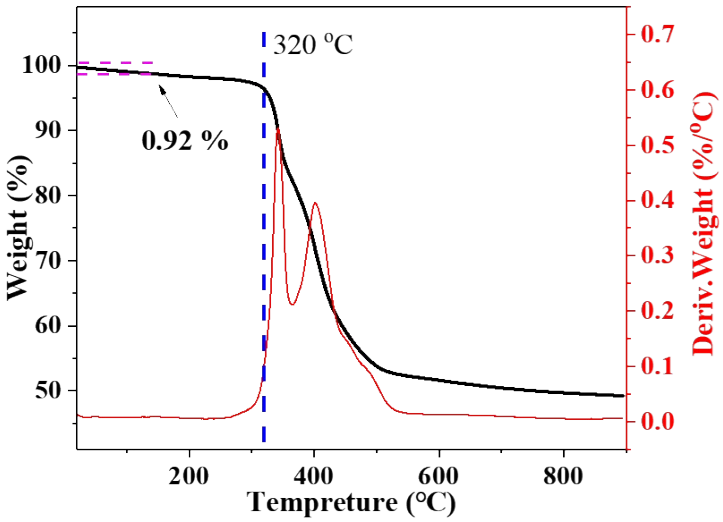

Fig. S4 Thermogravimetric curve of **Cu_{12}**

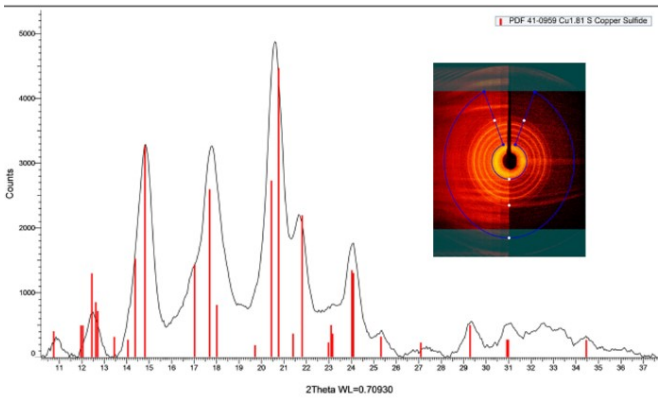

Fig. S5 The PXRD of the final decomposition from TGA

For investigating the thermal stability of **Cu_{12}**, the thermogravimetric analysis was carried out under an N_2 atmosphere from 20 to 900°C with a heating rate of 10°C min^{-1} **(Fig. S4)**. The weight loss is 0.92% below 100°C, which was close to the theoretical 0.63% of releasing one water molecule per **Cu_{12}**. The **Cu_{12}** can keep its skeleton before 320 °C. Then significant weight loss (49.2%) took place until the curve reached relatively stable. The residue was determined to be $Cu_{1.81}S$ according to PXRD analysis (**Fig. S5**).

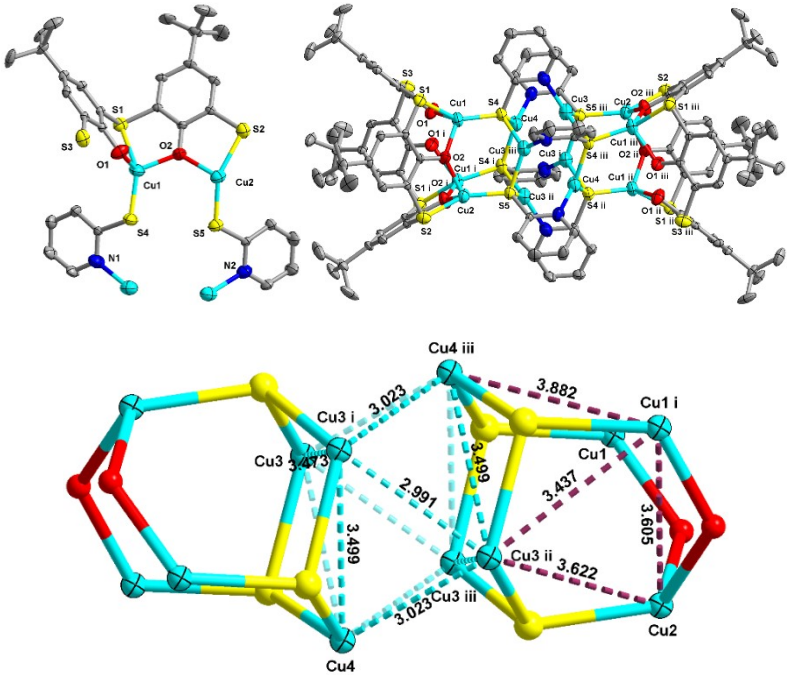

Fig. S6 Asymmetric unit and metal coordination environment of **Cu_{12}** (up) and Cu···Cu distance (Å) in Cu^{I}_{3}-HTC4A and "$Cu_6(2\text{-PyS})_6$" units (below).

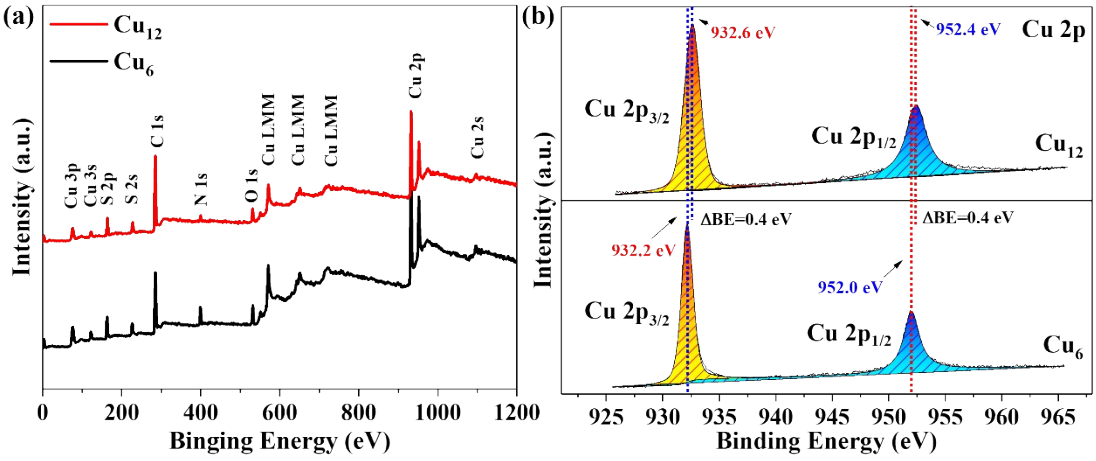

Fig. S7 (a) XPS spectrum and (b) High-resolution XPS spectra of Cu 2p for **Cu_{12}** and **Cu_6**.

XPS spectrum revealed the presence of the cluster components and the mono-valence nature of Cu centers. High-resolution XPS spectra of Cu 2p for **Cu_{12}** shifted to higher energy compared with that for **Cu_6**, which suggests that the electron density of Cu is lower in **Cu_{12}** than in **Cu_6**.

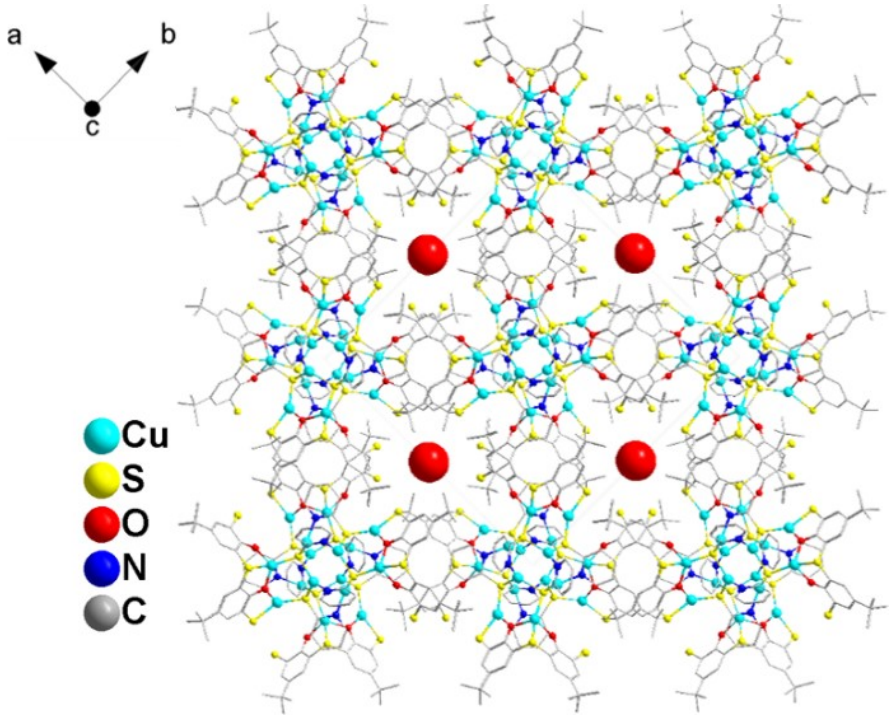

Fig. S8 The packing diagrams of **Cu_{12}** along the c-axis. The red ball represents the solvent H_2O in the crystal lattice

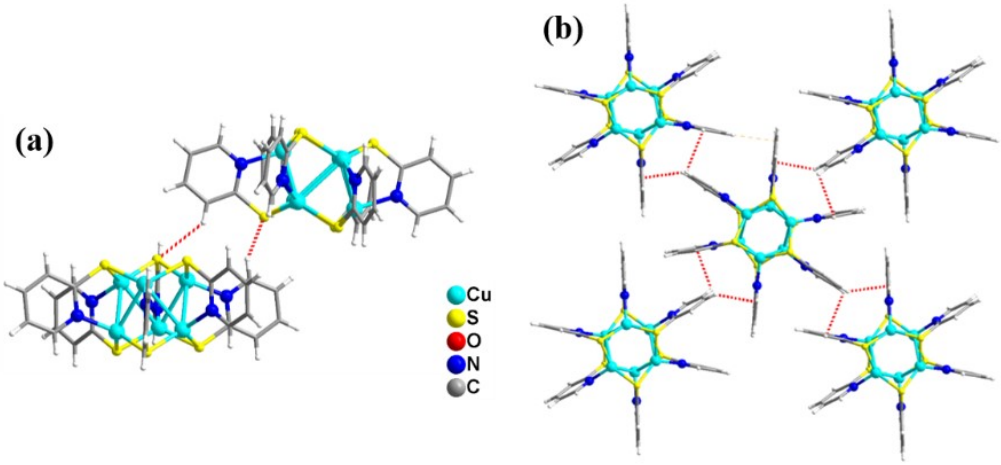

Fig. S9 Two kinds of interactions between **Cu_6** clusters

.

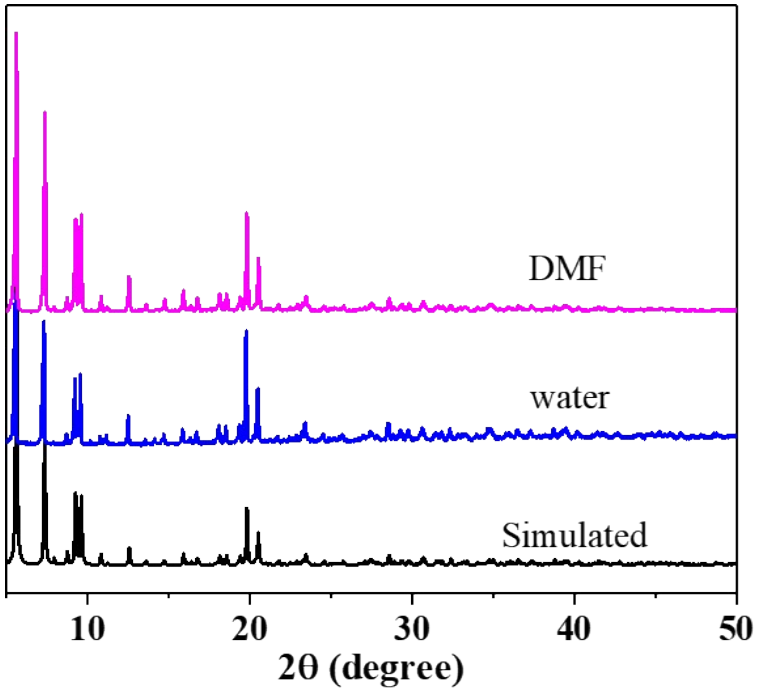

Fig. S10. PXRD pattern of $\mathbf{Cu_{12}}$ after the solvent photothermal experiments

Tables

Table S1. Crystal data and structural refinement parameters

Complex	**Cu_{12}**	**Cu_6**
formula	$C_{110}H_{118}N_6Cu_{12}O_9S_{14}$	$C_{30}H_{24}Cu_6N_6S_6$
Formula weight	2877.40	1042.15
Crystal system	tetragonal	monoclinic
space group	*P* 4_2/*m b c* (No.135)	*P 21/n* (No.14)
a(Å)	22.2481(9)	9.5857(8)
b(Å)	22.2481(9)	16.0466(11)
c(Å)	24.0155(12)	12.2754(10)
α(°)	90	90
β(°)	90	108.900(2)
γ(°)	90	90
Volume(Å^3)	11887.1(11)	1786.4(2)
Z	4	2
Temperature(K)	296(2)	296(2)
*D*c(g/cm^3)	1.608	1.937
μ(mm^{-1})	2.401	3.891
Reflections collected	51587	26990
Unique data	5411	3642
R_{int}	0.0820	0.0644
GOF on F^2	1.067	0.993
[a]R_1 [I>2sigma(I)]	0.0469	0.0304
[b]wR_2	0.1231	0.0795

[a]$R_1 = \Sigma||F_0|-|F_c||/\Sigma|F_0|$; [b]$wR_2 = \{\Sigma[w(F_0^2-F_c^2)^2]/\Sigma[w(F_0^2)^2]\}^{1/2}$

Table S2 The selected bond lengths (Å) for **Cu_{12}**

Bond	Distance	r	Value	Bond	Distance	r	Value
Cu1-O2	1.992 (3)	1.679	0.429	Cu2-O2^{i}	2.061 (3)	1.679	0.356
Cu1-O1	2.111 (4)	1.679	0.311	Cu2-O2	2.061 (3)	1.679	0.356
Cu1-S4	2.1732 (14)	1.86	0.429	Cu2-S5	2.176 (2)	1.86	0.426
Cu1-S1	2.3409 (15)	1.86	0.273	Cu2-S2	2.310 (2)	1.86	0.296
valence			1.442	valence			1.434
Bond	Distance	r	Value	Bond	Distance	r	Value
Cu3-N1	1.995 (5)	1.61	0.353	Cu4-N2	1.985 (6)	1.61	0.363
Cu3-S5^{ii}	2.2394 (14)	1.86	0.359	Cu4-S4^{iii}	2.2474 (15)	1.86	0.351
Cu3-S4^{iii}	2.2434 (16)	1.86	0.355	Cu4-S4^{ii}	2.2474 (15)	1.86	0.351
valence			1.067	valence			1.065
Symmetry codes: (i) *x*, *y*, −*z*+1; (ii) −*x*+1, −*y*+1, −*z*+1; (iii) −*x*+1, −*y*+1, *z*							

Table S3 The selected bond angles for **Cu_{12}**

Band	Angles [°]	Band	Angles [°]
O2-Cu1-O1	104.15 (15)	Cu3^{iii}-S5-Cu3^{ii}	101.67 (8)
O2-Cu1-S4	118.57 (11)	C1-O1-Cu1	116.9 (3)
O1-Cu1-S4	106.45 (11)	C7-O2-Cu1	116.6 (3)
O2-Cu1-S1	87.60 (11)	C7-O2-Cu2	117.0 (3)
O1-Cu1-S1	84.77 (10)	Cu1-O2-Cu2	125.55 (17)
S4-Cu1-S1	146.45 (6)	C25-N1-Cu3	124.3 (4)
O2^{i}-Cu2-O2	96.1 (2)	C21-N1-Cu3	117.7 (4)
O2^{i}-Cu2-S5	112.47 (11)	C26-N2-C30	117.0 (7)
O2-Cu2-S5	112.47 (11)	C26-N2-Cu4	118.8 (5)
O2^{i}-Cu2-S2	86.84 (10)	C30-N2-Cu4	124.2 (6)

O2-Cu2-S2	86.84 (10)	C12^{i}-S2-Cu2	95.20 (17)
S5-Cu2-S2	149.87 (8)	C21-S4-Cu1	111.48 (18)
N1-Cu3-S5^{ii}	123.66 (15)	C21-S4-Cu3^{iii}	108.46 (18)
N1-Cu3-S4^{iii}	120.59 (15)	Cu1-S4-Cu3^{iii}	102.18 (6)
S5^{ii}-Cu3-S4^{iii}	113.66 (6)	C21-S4-Cu4^{ii}	108.19 (18)
N1-Cu3-Cu3^{iii}	86.32 (13)	Cu1-S4-Cu4^{ii}	122.82 (7)
S5^{ii}-Cu3-Cu3^{iii}	127.95 (4)	Cu3^{iii}-S4-Cu4^{ii}	102.36 (6)
S4^{iii}-Cu3-Cu3^{iii}	69.24 (4)	C26-S5-Cu2	116.6 (3)
N1-Cu3-Cu4^{ii}	87.60 (13)	C26-S5-Cu3^{iii}	108.52 (16)
S5^{ii}-Cu3-Cu4^{ii}	69.23 (5)	Cu2-S5-Cu3^{iii}	110.25 (6)
S4^{iii}-Cu3-Cu4^{ii}	128.59 (5)	C26-S5-Cu3^{ii}	108.52 (16)
Cu3^{iii}-Cu3-Cu4^{ii}	71.15 (3)	Cu2-S5-Cu3^{ii}	110.25 (6)
N2-Cu4-S4^{iii}	122.62 (5)	S4^{iii}-Cu4-Cu3^{iii}	68.55 (4)
N2-Cu4-S4^{ii}	122.62 (5)	S4^{ii}-Cu4-Cu3^{iii}	126.50 (6)
S4^{iii}-Cu4-S4^{ii}	113.49 (8)	Cu3^{ii}-Cu4-Cu3^{iii}	70.10 (4)
N2-Cu4-Cu3^{ii}	86.58 (14)	C12-S2-Cu2	95.20 (17)
S4^{iii}-Cu4-Cu3^{ii}	126.50 (6)	C8-S1-Cu1	93.36 (17)
S4^{ii}-Cu4-Cu3^{ii}	68.55 (4)	C6-S1-Cu1	95.80 (17)
N2-Cu4-Cu3^{iii}	86.58 (14)	C6-S1-Cu1	95.80 (17)

Symmetry codes: (i) $x, y, -z+1$; (ii) $-x+1, -y+1, -z+1$; (iii) $-x+1, -y+1, z$.

Table S4 Some recent reports on Cu-based coordination compounds/representative composites for photothermal conversion

Compounds	Light source	Sample status	Heating rate	Maximum temperature	Stability	Reference
Cu_{12}	660 nm laser 0.4 W/cm^2	solid	9.5 °C/s in the first 5 s	124.5 °C	recyclable	**This work**
		30 mg/mL in H_2O	3.7 °C/min 1.0 °C/min (H_2O) in the first 10 min	59.3 °C 33.8 °C (H_2O)	-	
		30 mg/mL in DMF	4.8 °C/min 2.3 °C/min (DMF) in the first 10 min	67.9 °C 45.1 °C (DMF)	-	
$Cu^I_4Cu^{II}$	Xenon lamp 300 W	solid	1.49 °C/min in the first 10 min	46.3 °C	-	*Inorg. Chim. Acta*, 2023, **545** 121270
$Cu^I_6Cu^{II}_3$			1.95 °C/min in the first 10 min	49.6 °C	-	
$Cu^{II}_6Cu^I_3$	Simulated sunlight 0.1 W/cm^2	solid	4.48 °C/min in the first 10 min	78.2 °C	-	*Inorg. Chem*., 2023, **62**,401−407
$Cu^I_4Cu^{II}$-Ia	xenon lamp 300 W	solid	3.85 °C/min in the first 10 min	60 °C	-	*Dalton Trans*., 2022, **51**, 6053
$Cu^I_4Cu^{II}$-Ib					-	
$Cu^I_4Cu^{II}$-Ic			2.71 °C/min in the first 10 min	49.0 °C	-	
$Cu^I_4Cu^{II}$-Id			3.85 °C/min in the first 10 min	60 °C	-	
$Cu^I_4Cu^{II}$-IIa					-	
$Cu^I_4Cu^{II}$-IIb			4.63 °C/min in the first 10 min	69.8 °C	-	
$Cu^I_4Cu^{II}$-IIc			3.85 °C/min in the first 10 min	60 °C	-	
$Cu^I_4Cu^{II}$-IId					-	

Cu^{II}-1	Xenon lamp 300 mW	solid	1.8 °C/min from the beginning	28 °C	-	*Inorg. Chim. Acta*, 2021, **526**, 120531
Cu^{II}-2			1 °C/min from the beginning	27 °C	-	
Cu^{II}-3			2 °C/min from the beginning	32 °C	-	
Cu^{II}-1	Xenon lamp 300 mW	solid	2 °C/min from the beginning	40 °C	-	*Inorg. Chim. Acta*, 2020, **508**, 119608
Cu^{II}-2			0.9 °C/min from the beginning	37 °C	-	
Cu^{II}-3			1.5 °C/min from the beginning	36 °C	-	
SD/Ag_{18}a	808 nm laser 0.35 W/cm^2	solid	84.3 °C/s in the first 4 s	360 °C	destroyed	*Angew. Chem. Int. Ed.*, 2022, **61**, e202200823
	808 nm laser 5.0 W/cm2	300 μM in DMF	5.6 °C/min in the first 5 min.	51 °C	recyclable	
Ag_{155}	660 nm laser 0.1 W/cm^2	240 μM in DMF	7.82 °C/min in the first 5 min.	59.1 °C	recyclable	*Angew. Chem. Int. Ed.*, 2022, **61**, e202206742
{Mo_{154}}@CDC	808 nm laser 1 W/cm^2	0.204 mM in H_2O	8.4 °C/min in the first 5 min.	67 °C	recyclable	*Science Advances*, 2021, **7**, eabf8413
$PMo_{10}V_2$@TMB_{CT}	808 nm laser 1 W/cm^2	3.85 mg/mL)	7.0 °C/min in the first 4 min.	55 °C	recyclable	*Chem. Eng. J.* 2022 **446**, 137134
W-POM NCs	808 nm laser 2.0 W	300 mM in H_2O	10 °C/min in the first 3 min.	55 °C	recyclable	*ACS Nano* 2020, **14**, 2126−2136
rPOMs@MSNs@copolymer	808 nm laser 1.8 W/cm^2	1.0 mg/mL in H_2O	1.85 °C/min in the first 10 min	43.5 °C	-	*Adv. Healthcare Mater.* 2018, **7**, 1800320
$W_{18}O_{49}$	980 nm laser 0.72 W/cm^2	3.0 mg/mL in H_2O	8.24 °C/min in the first 5 min.	61.2 °C	-	*Adv. Mater.* 2013, **25**, 2095–2100